Modelling and Optimization of Peroxide Pulp Bleaching Process

Jonas Christensen Strömgren

LUND
UNIVERSITY

Department of Automatic Control

MSc Thesis
TFRT-6120
ISSN 0280-5316

Department of Automatic Control
Lund University
Box 118
SE-221 00 LUND
Sweden

Printed in Sweden by Tryckeriet i E-huset
Lund 2020

Abstract

The wood pulp industry has been around for a long time, but new higher quality pulp require more advanced solutions to old processes. One of these processes is the peroxide (PO) bleaching process, which is the last of a whole chain of bleaching processes at the Mörrum pulp processing plant. The aim of this thesis was to develop and study a model for the peroxide pulp bleaching process, and thereafter optimize the process with the model. The PO-stage is a multivariable, non-linear process with a variable retention time of a few hours. The models tested was a kinetic reaction model, a Gaussian process regression (GPR) model and hybrid models of the two. Before the models could be tested a retention time estimation model was made to compensate for the variable retention time. The bleaching simulations showed the kinetic model could not accurately model the brightness output. The kinetic lacked variability in the maximum brightness parameter C_∞. However, the combination of estimating C_∞ for the kinetic model with an GPR model proved to be a good performing model. Prediction on slow brightness changes was accurate, but fast changes was harder and large error could occur. The optimization of the hybrid model showed that chemical dosages could be lowered while achieving a smoother and more precise brightness. Further studies on robustness of the brightness model and the optimization model are needed before implementation on the real process can be done.

Acknowledgements

First and foremost I would like to thank my two supervisors. Sara Ingves for being a tremendous help during the time at Södra. Tore Hägglund at LTH for all the help on how to tackle a project like this and helpful advice writing the report. I would also like to extend my gratitude to Södra and all the people there for helping with the thesis and for the friendly company during coffee breaks.

Contents

1

Introduction

As sustainability becomes more important to consumers and manufacturers alike, sustainable resources are needed in areas they previously weren't. Wood pulp is one of those. A large part of producing pulp of good quality is bleaching the pulp, specifically the removal or breakdown of lignin. Lignin is part of what holds wood together but has a negative effect on paper quality and darkens it. Cooking the pulp removes some of the lignin while the rest has to be removed using chemical bleaching. The bleaching process consists of several stages of different bleaching chemicals with washing. Whilst all stages require some form of control system, the hydrogen peroxide stage (PO) is particularly complex [Dence and Reeve, 1996] and therefore, the focus of this thesis.

This thesis was conducted with the help from Södra Cell at their pulp plant in Mörrum. The Mörrum plant has two pulp lines: Premium paper pulp and dissolving pulp. Both lines have a similar structure and produces pulp of the kraft type, but differs slightly in brightness and strength requirements. The PO stage studied in this thesis is at the end of the premium paper pulp line.

Currently there is no model or control system implemented for the PO stage at the Mörrum plant. Instead, the chemical quantities are manually controlled by an experienced operator.

1.1 Problem Formulation

The PO stage process begins when the pulp is mixed with hydrogen peroxide and sodium hydroxide, before slowly flowing upwards through a large bleaching tower. Next, the pulp goes through another colder tower, where the chemical process is continued but at a very slow pace.

The PO stage is a multivariable, non-linear process with a 4-5 hour long retention time, which is the amount of time the pulp spends in the PO stage. This presents a need for more advanced control strategies that predict the behaviour of the system using a mathematical model. Read Section 2.1 for a more in depth description and analysis of the process.

1.2 Aims and Objectives

The initial aim was to properly model and optimize the PO process. After studying the process and reading studies [Alberth, 2011][Roberts et al., 2013][Jiang et al., 2019] on similar processes more explicit objectives were formulated:

- Test the kinetic bleaching model presented in [Alberth, 2011].
- Test Gaussian process models on the process.
- Using Gaussian process models, identify important input features for predicting output brightness.
- Combine the two models and test the resulting hybrid model on the process.
- Optimize the best performing model for brightness and chemical usage.

The last aim of optimizing the process with the model was left very open to focus more on the modelling part and to simply showcase the possible usage of the model.

1.3 Related Work

Whilst some studies have been done on peroxide bleaching, most focus on the lower brightness mechanical pulp instead of the high quality and high brightness kraft pulp. One such study was done by [Roberts et al., 2013], in which they applied a Gaussian Process Model coupled with an MPC controller. While their results indicated successful optimization of the chemical dosage, they did not disclose the exact performance of their model, and thus it's difficult to use as a benchmark.

Additionally, a study done on a steel plant process [Jiang et al., 2019] was very influential to the modelling approach of this thesis. Similarly it used a combination of Gaussian processes and linear regression to model the process. Lastly, another significant study [Alberth, 2011] implemented a kinetic chemical model to an equivalent peroxide bleaching process at a sister mill to Mörrum. This has very useful information about the PO bleaching process and the kinetic chemical model is used in the models here.

1.4 Outline

Chapter 2 starts off with an overview of wood pulping process and the chemical formulation of peroxide bleaching. The chapter continues with a short presentation of a kinetic bleaching model and Gaussian process regression models. Chapter 3 covers how the models are implemented, retention time estimation and chemical optimization. The results of all the models are shown and discussed in Chapter 4. Lastly, Chapter 5 wraps up the thesis with conclusions and suggestions of future work on the subject.

2

Background

2.1 Wood Pulp

The process of making paper pulp from wood is simply to separate the cellulose fibers from lignin and hemicellulose, which bind the cellulose together. What remain is a mass of shorter unconnected cellulose fibers. There are two main ways of cellulose separation: Mechanical pulping and chemical pulping. After pulping, the pulp is bleached depending on the brightness requirements of the final product.

Mechanical pulping, as the name implies uses mechanical forces to break down the wood into its constituents. While this is a very energy-demanding process, it produces a high yield compared to other processes. Another downside is the cellulose fibres are also damaged/cut, thus resulting in shorter fibres and weaker pulp.

On the other hand, chemical pulping produces stronger pulp with longer fibres at a lower yield. By combining heat and chemicals in stages the lignin is broken down into water-soluble molecules. Between the chemical stages the pulp is washed, removing leftover chemicals and lignin.

The process at the Mörrum plant is a chemical pulping process known as kraft pulping (or the sulfate process). Kraft pulping produces high quality pulp by removing most of the lignin, but not too much to weaken the pulp. However, the remaining lignin darkens the pulp, which is not desirable. Thus, additional brightening is required.

Kraft Pulp Bleaching

Bleaching of wood pulp can be divided into two categories: Dissolving lignin (delignification) and brightening. Kraft plants use a combination of the two in several stages. Delignification is done in the early stages and brightening in the later.

In kraft pulping the main delignification process is done by boiling the pulp with the chemical bleaching mixture called white liquor. Consisting of NaOH and Na_2S, the white liquor breaks down the lignin. To monitor pulp qualities and the delignification process, the Kappa number is used. The Kappa number is an approximation of the lignin content. Therefore, the Kappa number are used to determine the amount of bleaching agents needed to reach a certain brightness. The value

of Kappa ranges from 1-100, but can in certain circumstances exceed 100. Higher Kappa means higher lignin content, and thus higher chemical dosages are needed. How the Kappa number is measured is determined by the ISO 302:2015 standard. However, after the delignification stages the pulp usually has a very low Kappa number (9-14), making it unreliable and difficult to use further as the pulp brightens. Instead, the later stages uses the diffuse blue reflectance factor, ISO brightness (ISO 2470-1:2016), as quality control.

Brightening stages only break down the colored lignin (chromophore groups) to non-colored and causes minimal changes to the pulp strength and quality. This thesis focuses on one of the last bleaching stages at the plant, peroxide bleaching (PO).

Peroxide Bleaching A peroxide bleaching stage has two main benefits over other methods. The end brightness is more stable and no chlorine is used. However, peroxide bleaching has a few demanding requirements: Long reaction-time, high temperature, high pH, no heavy metal ions in the pulp and in some cases high pressure.

Process Description

This section offers a description of the process from a control system perspective and what challenges it presents in regards to modelling. Figure 2.1 shows a simplified chart of the process. In the figure, retention and dead time are used interchangeable as they are the same for this process. Dead time is mostly used in control settings and signifies the time between a change in controller output (H_2O_2 and NaOH dosages) and measured response of the process variable (pulp brightness).

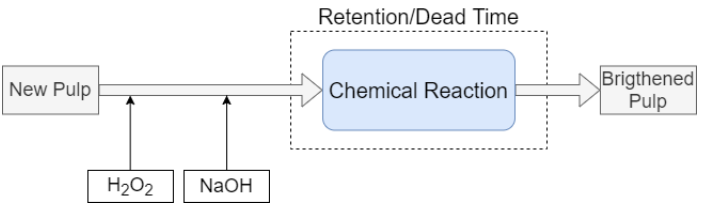

Figure 2.1 Simplified schematic of the peroxide bleaching process.

A long dead time causes problems for standard control solutions, as it need to predict the future output of the process. That the dead time is variable does not change the complexity of controlling the process significantly. Although, it does add the need for a retention/dead time prediction, which can further add to the uncertainty of predicting the process output.

Additionally, a long dead time can add one more complication. If the dynamics of the process change they will not show up in the process output until after the dead time. For the peroxide bleaching process the dynamics of the chemical reaction are dictated by the pulp properties, specifically how bleachable the pulp is.

With the problems mentioned above, the PO-stage modelling can be split into two parts:

- The nominal chemical reaction of the peroxide bleaching process.
- The change in bleachability as the pulp properties change with new pulp coming into the process.

Later in Section 3.4 this partition of the modelling is apparent in the use of a unique model for each part.

Table 2.1 show the important variables to the process and where they are measured during the PO-stage. The variables that are measured before (B) the process, can be used in PO-stage models as inputs. The variables measured during (D) the process can also be used as inputs, but there is an uncertainty to where they are measured during the dead time.

Table 2.1 The table highlights the important variables of the peroxide bleaching process and where they are measured by a sensor. The sensor positions are divided into Before B, During D and After A the process.

Type	Variable	Sensor Positions
Process Variable	Brightness	B A
Control	$[H_2O_2]$ Dosage	B
Output	$[OH^-]$ Dosage	B
Other measurements	Temperature	B D
	Kappa	B
	Fiber length	B A
	pH	D
	Pulp concentration	B A
	Pressure	D
	$[OH^-]$ Concentration	D
	$[H_2O_2]$ Concentration	D
	Pulp Flow	B A

Chemical Reactions The active bleaching chemical in the peroxide stage is the hydrogen peroxide ion (OOH^-), which attacks the chromophore groups, breaking them down to non-colored groups. Otherwise, the process preserves the lignin and the structural strength of the pulp. A complication when using peroxide bleaching is producing the highly reactive hydrogen peroxide ions. Currently, hydrogen peroxide (H_2O_2) and sodium hydroxide (OH^-) are mixed into the pulp to react and produce the hydrogen peroxide ions. The chemical reaction equation of hydrogen peroxide ions is shown below,

$$[H_2O_2] + [OH^-] \longleftrightarrow [OOH^-] + [H_2O]. \tag{2.1}$$

Here brackets signify the concentration of the enclosed molecule. The chemical equilibrium for the reaction above has been studied by [Teder and Tormund, 1980], who formulated the following equation

$$K_E = \log_{10} \frac{[HO_2^-]}{[OH^-][H_2O_2]} = \frac{1300}{T} - 2.13 + 0.15 \cdot \sqrt{[Na^+]}. \tag{2.2}$$

Here T is the absolute temperature. Whilst the equilibrium equation was designed mainly for lower temperatures $20 - 80$ C°, later studies by [Malmberg, 2006] also show that the equation is applicable to higher temperatures, which is the case for the peroxide stage at the Mörrum plant.

2.2 Kinetic Peroxide Bleaching Model

Several studies [Mota et al., 2007] have been done to model the chemical kinetics of peroxide bleaching. Eventually, the bleaching model from [Alberth, 2011] was chosen for this thesis. Her model is an adaptation of a model presented in [Malmberg, 2006]. [Alberth, 2011] did her study on the sister mill of Mörrum, Värö pulp mill. This is the main reason for choosing her model for this thesis, as the PO-stage of the two mills are similar in design and specifically in available measurements. Furthermore, the focus of her study was to validate and tune the different parts of the model using chemical laboratory experiments. Her method of study complements this thesis well, as the emphasis of this thesis is on modeling and optimizing using real mill data. Below is a short description of the model [Alberth, 2011] designed and tuned.

The kinetic bleaching model consists of three main differential equations, equations 2.3-2.5. These equations models the change in brightness and the peroxide and hydrogen concentrations respectively.

$$\frac{dC}{dt} = A_1 \cdot e^{\frac{-E_1}{R \cdot T}} \cdot \frac{K_C[HO_2^-]}{1 + K_C[HO_2^-]}(C - C_\infty) \tag{2.3}$$

$$\frac{d[H_2O_2]}{dt} = [H_2O_2] \cdot A_2 \cdot e^{\frac{-E_2}{R \cdot T}} \tag{2.4}$$

$$\frac{d[OH^-]}{dt} = ([OH^-] - A_3) \cdot e^{-E_3} \tag{2.5}$$

Additionally, to connect equations 2.4,2.5 to the brightness reaction equation 2.3 the reaction equilibrium equation 2.2 mentioned previously have to be used. It is reformulated to calculate the $[HO_2^-]$ and the equilibrium variable K_E is not restated.

$$[HO_2^-] = [OH^-][H_2O_2] \cdot 10^{K_E}. \tag{2.6}$$

Something to note in Equation 2.5 is the lack of pH measurement usage. However, Alberth showed in her thesis that pH is a poor estimation of OH^- concentration. The reason, she theorized, being that pH only measures free H^+ ions and the pulp has a buffer for negative charged ions, like OH^- Her solution was to assume the exponential model in Equation 2.5 and do laboratory tests to fit the parameters A_3 and E_3.

Below, in Table 2.2, all the parameters used in the kinetic peroxide bleaching model, equations 2.3-2.6, are presented.

Table 2.2 Values of the parameters used in the kinetic model, identified by [Alberth, 2011].

Parameter	Value	Description
C_∞	$0.17\ \mathrm{m^2/kg}$	Minimum light absorption
K_C	$13.3\ (\mathrm{mol/l})^{-1}$	Concentration coefficient
A_1	$333 \cdot 10^6\ \mathrm{s^{-1}}$	Reaction speed
A_2	$1.8 \cdot 10^{11}\ \mathrm{s^{-1}}$	
A_3	$0.013\ \mathrm{mol/l}$	
E_1	$70.1\ \mathrm{kJ/mol}$	Reaction activation energy
E_2	$99\ \mathrm{kJ/mol}$	
E_3	$5.2\ \mathrm{s^{-1}}$	
R	$8.3144\ \mathrm{J \cdot K^{-1}/mol^{-1}}$	Universal gas constant
T	K	Temperature

ISO-Brightness

The mill were using ISO reflectance R as the brightness measurement while the model uses the brightness absorption coefficient C_K. Equation 2.7, shown below, converts R to C_k and can easily be reversed.

$$C_K = s \cdot \frac{(1-R)^2}{2 \cdot R} \tag{2.7}$$

Here light scattering coefficient s is not known, but [Alberth, 2011] calculated an average value for s over several laboratory experiments. This average value is used in this thesis as the study done by [Alberth, 2011] is deemed close to equivalent in chemical properties and brightness values.

2.3 Gaussian Process Regression

The following section offers a short description of Gaussian Process Regression (GPR) models, for a more in-depth definition see [Rasmussen and Williams, 2006] or [Roberts et al., 2013]. GPR models main benefit over dynamic models is the ability to model a nonlinear process requiring very limited prior knowledge of the

process dynamics. GPR models belong to the group Bayesian non-parametric models, as they do not infer a set of parameters and use probability theory as their main tool. Before providing the definition of GPR models, the process problem itself needs to be set up. A typical regression problem can be described by

$$y_i = f(\mathbf{x}_i) + \varepsilon. \tag{2.8}$$

Here $\varepsilon \sim \mathcal{N}(0, \sigma_n^2)$ is white measurement noise, $\mathbf{x}_i$ is an input vector at time i, y_i is the output at time i and $f(\mathbf{x}_i)$ is the unknown process function. For the peroxide bleaching process $\mathbf{x}_i$ are a selection of measurement from Table 2.1, y_i is the output brightness (or another pulp property) and $f(\mathbf{x}_i)$ is the peroxide bleaching process. Inferring an approximation of the unknown process function $f(\mathbf{x}_i)$ is the goal of the GPR models. With an approximation of $f(\mathbf{x}_i)$, predictions of y_j can be made for new input vectors $\mathbf{x_j}$. How a GPR model is defined and can predict process outcomes is explained in the remainder of this section. However, first a short exploration of some probability theory concepts is appropriate.

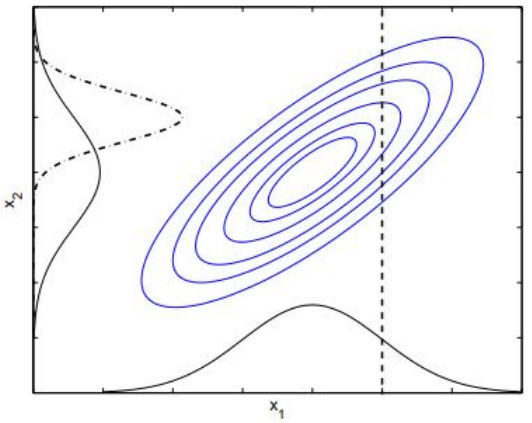

Figure 2.2 Here different probability distributions for two random variables are shown: The joint distribution (blue ellipsoids), the marginal distributions of both variables (black solid lines) and the conditional distribution (black dotted line) for x_2 when x_1's value is known. Picture taken from [Roberts et al., 2013].

The key concept of GPR models is conditional probability, which can simply be explained as knowledge of some random variable x_1 provides information of the probability of another random variable x_2. Figure 2.2 illustrates this concept using two Gaussian distributions x_1 and x_2. The blue ellipsoid figures represent the joint distributions $p(x_1, x_2)$ of the two variables, which is determined by their 2 x 2 covariance function and their mean values. The black solid line is the respective marginal distributions $p(x_1)$ and $p(x_2)$. The black dotted line is the conditional

distribution when the value of x_1 is known, $p(x_2|x_1) = known$. The conditional distribution shows how information of the covariance and the value of one variable can decrease the uncertainty of another variable. This thinking is the core of GPR models. GPR models can use data points to gain knowledge of the covariance and to then form conditional distributions to make predictions.

Describing how a Gaussian Process actually works, is difficult to do in a short and intuitive manner. Therefore, the reader is once again referred to [Rasmussen and Williams, 2006] for a complete explanation. However, one important property of Gaussian Processes, which is needed later, is that they can be fully defined by a mean function $m(\mathbf{x})$ and a covariance function $k(\mathbf{x}, \mathbf{x}')$.

Kernel

So far the GP covariance function has only been defined for a single data point, but it needs to work for many data points to gather as much information as possible. Therefore, the covariance function is defined over an arbitrary but finite number data points by introducing a covariance kernel function. The covariance kernel function is a way to store the covariance between arbitrary data points in a predefined manner. Thus, the GP can be extended to a complete training set of variables $(\mathbf{X}, \mathbf{y}) = \{(\mathbf{x}_i, y_i)|i = 1, 2, ..., n\}$. The kernel function is defined as

$$K(\mathbf{X}, \mathbf{X}) = \begin{pmatrix} k(\mathbf{x}_1, \mathbf{x}_1) & k(\mathbf{x}_1, \mathbf{x}_2) & \cdots & k(\mathbf{x}_1, \mathbf{x}_n) \\ k(\mathbf{x}_2, \mathbf{x}_1) & k(\mathbf{x}_2, \mathbf{x}_2) & \cdots & k(\mathbf{x}_2, \mathbf{x}_n) \\ \vdots & \vdots & \ddots & \vdots \\ k(\mathbf{x}_n, \mathbf{x}_1) & k(\mathbf{x}_n, \mathbf{x}_2) & \cdots & k(\mathbf{x}_n, \mathbf{x}_n) \end{pmatrix}. \tag{2.9}$$

Since only $\mathbf{y}$ is available for the training set, the measurement noise $\varepsilon \sim \mathcal{N}(0, \sigma_n^2)$ have to be incorporated.

$$\text{cov}(\mathbf{y}) = K(\mathbf{X}, \mathbf{X}) + \sigma_n^2 I \tag{2.10}$$

A common kernel function is the Squared Exponential (SE) kernel, also called Radial Basis or Gaussian Kernel. The SE kernel can model several smooth nonlinear functions and has the property of being infinitely differentiable.

$$k_{SE}(\mathbf{x}, \mathbf{x}') = \sigma^2 \text{exp}\left[-\left(\frac{\mathbf{x} - \mathbf{x}'}{\lambda} \right)^2 \right] \tag{2.11}$$

Here the SE kernel introduces two hyperparameters σ and λ. How these are determined will be explored later in Section Hyperparameter Optimization. λ is the length scale hyperparameter, which determines how fast the function changes. If the input $\mathbf{x}$ is a vector then λ can also be a vector with equal length to $\mathbf{x}$.

Prediction

After conditioning on the training set $(\mathbf{X}, \mathbf{y})$, the GPR model is ready to predict on a test set $(\mathbf{X}_*, \mathbf{y}_*)$. Here $\mathbf{y}_*$ is the so far hidden measurement. However, as $\mathbf{y}_*$ includes measurement noise, it isn't interesting to predict. Instead the prediction objective is the underlying problem function $\mathbf{f}_* = f(\mathbf{X}_*)$. Thus, a joint covariance function is formed with the prior and the test set.

$$\operatorname{cov}\begin{pmatrix}\mathbf{y}\\ \mathbf{f}_*\end{pmatrix} = \begin{pmatrix}K(\mathbf{X},\mathbf{X}) + \sigma_n^2 I & K(\mathbf{X},\mathbf{X}_*)\\ K(\mathbf{X}_*,\mathbf{X}) & K(\mathbf{X}_*,\mathbf{X}_*)\end{pmatrix} \tag{2.12}$$

Finally, the predictive equations can be written as

$$\mathbf{f}_*|\mathbf{X},\mathbf{y},\mathbf{X}_* \sim \mathcal{N}(\bar{\mathbf{f}}_*, \operatorname{cov}(\mathbf{f}_*)), \tag{2.13}$$

$$\bar{\mathbf{f}}_* \triangleq \mathbb{E}[\mathbf{f}_*|\mathbf{X},\mathbf{y},\mathbf{X}_*] = K(\mathbf{X}_*,\mathbf{X})[K(\mathbf{X},\mathbf{X}) + \sigma_n^2 I]^{-1}\mathbf{y}, \tag{2.14}$$

$$\operatorname{cov}(\mathbf{f}_*) = K(\mathbf{X}_*,\mathbf{X}_*) - K(\mathbf{X}_*,\mathbf{X})[K(\mathbf{X},\mathbf{X}) + \sigma_n^2 I]^{-1}K(\mathbf{X},\mathbf{X}_*). \tag{2.15}$$

One thing to note is even if the GP's prior mean function is set to zero, the posterior prediction mean is not necessarily zero.

Explicit Basis Function

For regression problems the GP model can be extended to include basis functions $h(\mathbf{x})$ and basis function coefficients β, as

$$g(\mathbf{x}) = h(\mathbf{x})^T \cdot \beta + f(\mathbf{x}). \tag{2.16}$$

The basis function can be seen as an replacement to the mean function of the GP. However, basis functions can express a wide range of functions. For example, set $h(\mathbf{x}) = [1\ \mathbf{x}]^T$ and the basis function with coefficients can act as linear regression. The basis function is most important when predicting far from observations where most of the kernel functions have little to no impact.

Hyperparameter Optimization

To make the most out of a GP model, the hyperparameters needs to be inferred. A common way is by maximising the likelihood $P(\mathbf{y}|\mathbf{X})$ over the hyperparameters: β from the basis function, σ^2 and λ from the kernel function. This can be written as

$$\hat{\beta}, \hat{\sigma^2}, \hat{\lambda} = \underset{\beta,\sigma^2,\lambda}{\arg\max} \log P(\mathbf{y}|\mathbf{X},\beta,\sigma^2,\lambda). \tag{2.17}$$

This optimization can be very computational heavy as it scales as $O(k \cdot n^3)$, where k is number of function evaluations and n is the number of observations. While there exists faster sparse fitting methods, they will not be discussed here and the reader is referred to the documentation of the Statistics and Machine Learning Toolbox of Matlab.

3

Methodology

3.1 Retention Time Model

Estimation

Knowledge of the retention time is crucial for tuning and implementing the bleaching model. Otherwise, the pairing of in- and out-data becomes inaccurate and the bleaching model will not function. Figure 3.1 provides an overview of the PO stage, excluding a few small external flows. The kinetic model needs the PO250 retention time, but the measurements are made at point A and B. Therefore the retention time model needs to estimate the retention time for PO250 and from point A to B. The time spent in pipes and washer presses were assumed to be inconsequential compared to time in PO250 and T260.

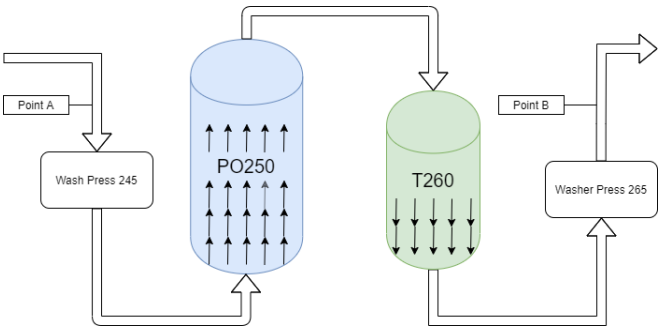

Figure 3.1 Simplified flowchart of the PO-stage. Point A and B are the sensor stations for the vital measurements of process. The blue cylinder is the PO250 tower, were the majority of the bleaching occurs. The green cylinder is the T260 tower, which mainly acts a reserve in case of differing production speeds before and after the stage. Washer press 245 and 265 washes the pulp mixture from chemicals.

A pre-existing retention time prediction was already implemented for the plant, however the existing model had a number of issues. First, the pre-existing model

is a prediction, and therefore it assumes the time current in-/outflow will remain constant. Any disturbances or quick temporary changes to the in-/outflow would be extrapolated and dictate the retention time estimation. Second, the calculations of the T260 outflow seemed to be missing some additional small external flows. Thus, a more accurate retention time model were needed.

[Lenz et al., 2005] used a Kalman Filter for estimating the retention time. However, there are certain problems of applying one for this thesis. The main one is imprecise and noisy volume measurement of the T260 tank, rendering any estimation of the in-/outflow useless. Thus, the estimation in this thesis is done without the volume measurement of the T260 tank. Without the sensor fusion of volume measurement and outflow, the Kalman filter was deemed obsolete.

Integration of outflow In order to calculate the retention time of a container, two measurements are needed: The volume flowing out and the volume in the container. With that, an integration of the outflow is made backwards until the volume in the container is reached. The equation of volume integration follows as

$$V(t) = \int_{t-t_{ret}}^{t} O_v(s)ds. \tag{3.1}$$

Here $V(t)$ is the volume at time t, t_{ret} is the wanted retention time and $O_v(s)$ is the volume flow at time s. However, as the measurements of time, flow and volume are discrete, summation instead of integration is used.

$$V_t = \sum_{i=t-t_{ret}}^{t} O_{v,i} \tag{3.2}$$

First, the inflow is estimated using pulp concentration and flow measurement at Point A and concentration measurement before the PO-reactor. This is possible as the pulp flow is the same for both concentration measurements. This is important as the concentration is $3-4$ times higher after Washer Press 245 than before. Thus, the inflow to PO250 is $0.25-0.3$ of the flow at Point A.

The pulp concentration measurements show noisy and unreliable behaviour when comparing values of pulp mass production across the line. So, an average of the amount of mass flow was taken from before and after the PO-reactor, decreasing the disturbances from measurements noise.

As the pulp mass flows upwards in the PO-reactor a decrease in pressure is measured. While the expansion of the fluid can be ignored, some oxygen gas has been added which will expand as the pressure decreases. Expansion of the pulp mass increases the volume of the flow and thus the retention time decreases. To counteract this disturbance an adjustment to the inflow volume has been added to the retention time integrator. The adjustment is made by calculating the density of the pulp mass flowing through the tower and knowledge of the weight of the pulp mass before the tower. Density is determined using two pressure measuring points along the height the tower.

$$I_{we} = I_{pulp} + I_0 \cdot (1 - C_{in}) \tag{3.3}$$

I_{we} (kg/s) is the inflow weight, I_{pulp} (kg/s) is the pulp inflow weight, I_0 (l/s) is the original inflow volume and C_{in} is the pulp concentration.

$$I_v = \frac{I_{we}}{\rho} = -I_{we}\frac{g \cdot \Delta h}{\Delta P} \tag{3.4}$$

I_v (l/s) is the new adjusted inflow volume, ρ (kg/m^3) is the mean density of the inflow, ΔP is the pressure difference, g is the gravitational constant and Δh is the height between pressure measuring points.

A major issue for estimating the retention time is the lack of accurate methods to validate the estimation. A crude validation can be made by observing the fiber length before and after the PO-bleaching stage. Change in fiber length is mostly due to change of wood type. Measuring the time between before and after the PO-tank for large step changes in fiber length, a retention time can be estimated. However, the frequency of the sample time for fiber length is quite long and variable, so only a very rough estimate can be made.

A similar validation can be made for just the PO-retention time using peroxide inflow and peroxide concentration at the top of the PO-tower.

Prediction

To be able to predict accurately the retention time the future inflow/outflow have to be known. The inflow and outflow of the PO-tower and P2-tower is determined by the production speed of the whole bleaching stage. An operator sets the production speed manually based on the several factors earlier in the production. The chain of manually determined production speeds makes accurate prediction of the retention time very difficult and out of the scope of this thesis. Thus, the retention time was assumed to be known as accurately as the retention time estimation is in the section above.

3.2 Kinetic Model Implementation

The kinetic model is based on the differential equations 2.3-2.5, which need to be solved for the duration of the retention time. This problem is a non-stiff system of ordinary differential equations. The solver chosen is the built-in Matlab function ode45, which implements an explicit Runge-Kutta (4,5) method. Measurements needed for the solver are the starting values of the three differential equations as well as the retention time.

As mentioned in Section 2.2, the parameters of the kinetic model were fitted to a similar process at another plant. Also, the wood pulp properties can change from day to day based on the type of wood used. Therefore, a parameter fitting of those presented in Table 2.2 is needed at appropriate intervals.

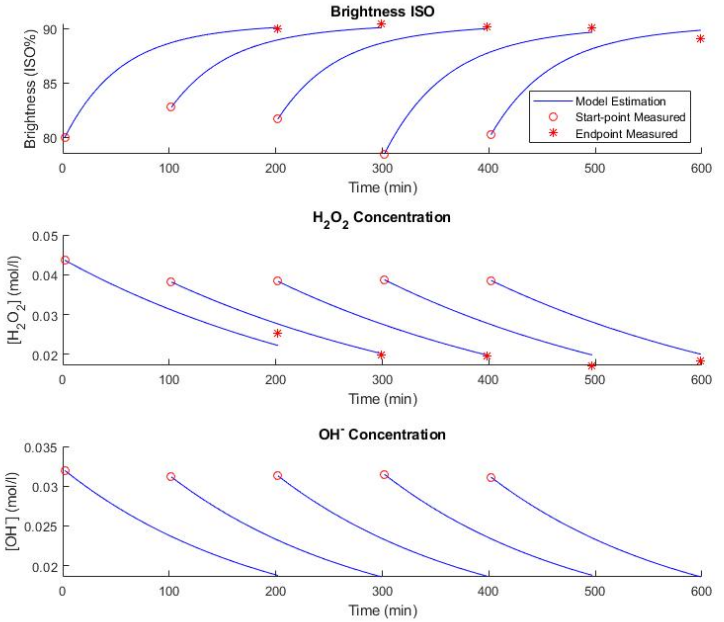

Figure 3.2 The three graphs show state values of the differential equations of the kinetic model, for five training data points. The blue lines represent the estimated state values, the red circles represent the measured starting point and the red dots represent the measured endpoints.

The parameter fitting was done with a trust-region-reflective least squares fitting method using the Optimization toolbox from Matlab. The algorithm works by choosing a starting point in the input space and simplifying the objective function to reflect the true function over a trust-region. Next, a new point in the input space is calculated by minimizing the objective function over the trust-region. If the new point in input space is unchanged, the trust-region is shrunk instead. The previous step are repeated to obtain an approximation of the minimized objective function [Coleman and li, 1994] [Coleman and Li, 1996]. In this application, the objective function is the norm error between the true values and the solver for the differential equations 2.3-2.5.The input space are the parameters in Table 2.2.

Figure 3.2 show how the states of the differential equations develop over time. The model was fitted for 20 data points, but only 5 are shown to obtain a better view of the differential dynamics. From the two top graphs it can be clearly seen that the model does not reach all the training endpoints. This was the case for all fittings of the kinetic model.

3.3 GPR Model Implementation

Implementing the GPR model was done using the built-in Matlab functions from the Statistics and Machine Learning Toolbox. The toolbox offers a number of different structural options for constructing a GPR model; however, the standard GPR model (as described in Section 2.3) was used for this thesis.

Nonetheless, several parameters and features needed to be determined to achieve an effective model. The remainder of this section describes how the the key parameters and features of the GPR models were determined. Section A.2 contains some additional parameters as well as the simulations done to determine the the parameter values.

Input Features

Deciding what input features to use from the data is a complex but crucial step to obtain high performance machine learning models. Feature selection can improve prediction precision and calculation speed. Knowledge of the process can also be gained by feature selection. A number of techniques and algorithms have been developed for this purpose, and choosing one for this process is not straightforward [Guyon and Elisseeff, 2003]. The feature selection method has to fit the type of model used. Otherwise, features selected could be of value but unusable by the model. Therefore, a more experimental approach was adopted.

GPR models have a built-in feature selection in the covariance kernel parameter optimization. The kernel scales λ, shown in Equation 2.11, functions as inverse weights for the model inputs. Along with the other hyperparameters, the kernel scales are optimized over the training data, as explained in Section 2.3. Therefore, by fitting a GPR model over a large part of the data, the importance of each input feature can be seen in the kernel scale.

The difficult part is to choose the right data points. Since the fitting a GPR can be computationally complex, there is a soft cap on the number of training data points. The GPR is also susceptible to overfitting when training data points are all very similar. Subsequently, the training data points were divided into two parts. The first part has 600 data points spread equally on half of complete data set, so much of the process dynamics are captured. The second part has 8 data points spread equally on the other half of the complete data set. This has the purpose of preventing overfitting. By introducing data points further apart, the algorithm assumes a higher uncertainty.

Subsequently, choosing input features under a certain kernel scale threshold, only a few simulations of the complete models are needed to determine which input features are best suited.

Training Set Selection

Similar to many other machine learning models the driving force of GPR models is the training data. As there is a practical limit to the number of data points, a selection has to be made. Simply selecting the most recent data is a valid option.

However, as the process has a long retention time, the most recent output is already as old as the retention time, and therefore less useful. Subsequently, recent data can be reinforced with data selected from older sets. Presented below are two different data selection methods. Both were used in testing the bleaching models described in Section 3.4.

Big Data The idea is to use a very large data set to capture as much diverse information as possible for the GPR models. Practically, this means selecting evenly spaced data points from the whole training set. More advanced selection of the individual data points would probably be advantageous, but was unfortunately passed over due to limited time.

K-means Clustering K-means clustering is a data partition algorithm with several applications in classification and machine learning training. K-means clustering partition a data set into a fixed number of subsets (clusters), each with a center. Next, the algorithm minimizes the total distance between all the data points to their closest center by moving the cluster centers. The data was also normalized so the input features would be equally important for the clustering algorithm.

The purpose for using K-means clustering in this study is to supply the GPR models with more specific data points. Because of the covariance kernel dependence on input distance (see Equation 2.16), only training data similar to the test data contributes to the prediction. As K-means clustering also uses distance to partition the training set, choosing the closest training data cluster to the test data should give more useful training data.

3.4 Hybrid Models

In this section the two hybrid models are presented. To the author's knowledge combining a machine learning and a more traditional model has not been done in a pulp bleaching setting.

An additional simple GPR model, which directly predicts the ISO brightness, was also constructed and tested in the simulations. It will not be described here, as its framework is rudimentary.

Absorption Floor Level Hybrid Model (C8 GPR)

A major issue with the kinetic model is the inference and use of the light absorption floor level coefficient C_∞, see Equation 2.3. C_∞ is dependent on the type of chromophore groups. A study done by [Peter and Manfred, 2006] divides chromophores into three groups: fast bleaching, slow bleaching and non-bleachable. However, that requires laboratory tests every time the pulp changes characteristics. As those laboratory tests were not available for this thesis, another approach was needed. Also, [Alberth, 2011] mentioned an improved dynamic inference of C_∞ for future studies would be of interest.

The main idea of this model is to use a GPR model to predict the C_∞ parameter at every timestep and then use the kinetic model with the estimated C_∞ to predict the brightness. However, training this model requires the "true" C_∞ to be calculated. Using the input $\mathbf{x}$, the end brightness y and the kinetic model, a "true" C_∞ can be solved for. Figure 3.3 illustrates the workflow of training and prediction using this model.

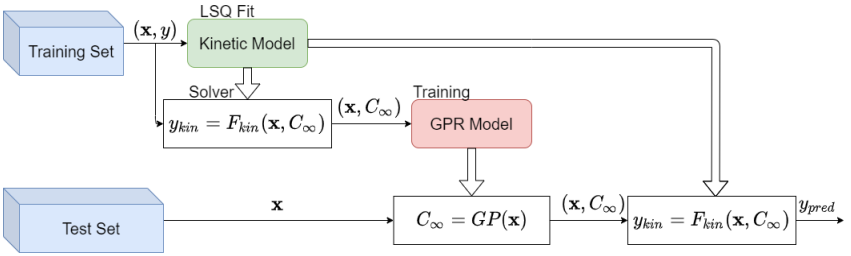

Figure 3.3 Flowchart of the absorption floor level GPR model.

A benefit and a potential problem of this model is that the GP tries to capture all the discrepancies between the kinetic model and process into the C_∞ parameter. This improves the accuracy of the model; however, it also limits the resulting kinetic model when optimizing.

Kinetic Error GPR Model

The concept of this model is to first use the kinetic model to predict the brightness output. Second, let the GPR model estimate the error of the kinetic prediction. Third, combine their predictions to obtain final brightness prediction. Figure 3.4 describes the structure of the model training and prediction.

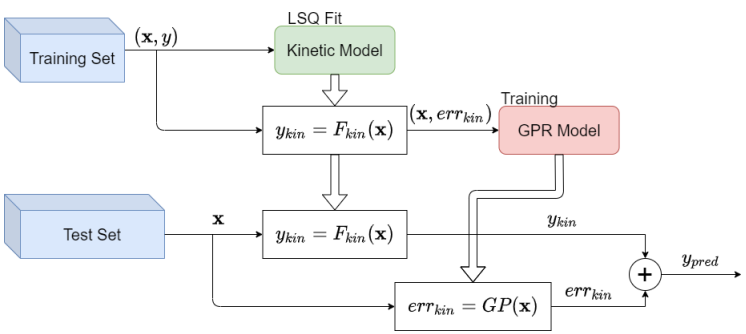

Figure 3.4 Flowchart of the kinetic error GPR model.

The concept of GPR models predicting the error of other models is not new, and has been used in studies in several fields of research [Chen et al., 2014] [Jiang et al., 2019].

3.5 Chemical Optimization

The dosage of the bleaching chemicals (hydrogen peroxide and sodium hydroxide) is responsible for the largest variance in brightness output and production cost in the PO-stage among the inputs. Therefore, improving the PO-stage process is done optimizing the chemicals. Similar studies [Roberts et al., 2013] [Taylor and Akida, 2007] have also focused on chemical dosage for bleaching optimization. Their method for optimization was Model Predictive Control (MPC), which uses quadratic optimization over a finite horizon step prediction of the model and control inputs. For this thesis MPC was not chosen for a couple of reasons. First, MPC only works with linear models. Nonlinear MPC exists but can be computationally heavy and linearizing the models could potentially result in loss in precision. Second, control inputs are only at the start of the bleaching process. This causes the control input at every time step of the prediction to be obsolete.

Instead, the goal attainment method was chosen as the optimization algorithm [Gembicki and Haimes, 1975] [López Jaimes et al., 2011]. The goal attainment method accepts a set of goals and a corresponding set of weights. This allows the algorithm to under- and overachieve the goals based on their weights. And crucially, the algorithm can handle nonlinear functions .

Implementation was done with the Optimization Toolbox from Matlab. The set of goals are the a fixed value brightness output, and low amounts of hydrogen peroxide and sodium hydroxide. Thus, by adjusting the weights, the algorithm can focus more on saving chemical costs or obtaining a smoother and higher brightness output.

Optimizing C8 GPR Model

In the interest of time, only one brightness model was chosen to apply the optimization. Section 4.3 presents the results which shows the reasons for choosing the C8 GPR model as the most suitable for optimization.

The optimization works by using the kinetic model with the predicted C_∞ that the C8 GPR model provides. The goal attainment method then uses the kinetic model with the $[H_2O_2]$ and $[OH^-]$ dosages as input variables to optimize the brightness. Afterwards, the brightness has to be estimated with the new chemical dosages. Using the original estimated C_∞ at that particular timestep, the kinetic model can make an estimation of the optimized output brightness. While this estimation of the optimized brightness will not be perfect, the results in Section 4.3 show that the no other model can accurately account for changes in chemical dosages.

4

Simulations and Analysis

Data Preparation and Statistics

To obtain better models and test them accurately, large amounts of data were needed. The data sets had to be carefully chosen to avoid any missing data input, caused by malfunctioning sensors. Also, the data should represent as much of the process dynamics as possible. Therefore, data sets which were similar in output were avoided.

Three time periods of 96 hours each were found to be complete and have varying degrees of output brightness variance. During testing, the time periods are slightly shorter than 96 hours, as the retention time causes a time shift. Also, all models require training data before making predictions, which further shortens the actual testing time period. The time interval between data points is one minute.

Performance Evaluation Metrics

To evaluate the performance of the models the Root Mean Square Error (RMSE) was used. RMSE penalizes large model errors. So even if the model predict accurately for some parts of the test set, few but large errors can increase RMSE substantially. This behaviour is wanted as large errors can potentially ruin the pulp quality or damage process equipment. RMSE is formulated as

$$\text{RMSE} = \frac{\sum_{i=1}^{N} \sqrt{(\mathbf{y}_i - \mathbf{y}_i^*)^2}}{N}. \tag{4.1}$$

Here $\mathbf{y_i^*}$ is the predicted output, $\mathbf{y_i}$ is the observed output and N is the number of data points of the prediction set.

4.1 Retention Time

Estimation and Validation

As explained earlier in Section 3.1, the pre-existing models for retention time prediction contained a number of issues, nevertheless they were once tuned originally

back in 1995 and could help validate the current model. Especially, pre-existing model for the PO retention time, which seems to have no clear model errors.

Another typical method for validation of retention time is to perform a step response. This could not be done at the plant at the risk of making the pulp unusable. Instead, a retention time was estimated by fitting an ARX model to the in- and outdata.

Figure 4.1 presents the results obtained from estimation of the retention times in two separate graphs: Top graph shows PO retention time and bottom graph shows the PO + T260 retention time, which is assumed to be the same as retention from point A to point B in Figure 3.1. A separate for T260 retention were omitted, as the kinetic model does not require it and there are no valid input-output pairings to fit an ARX model to.

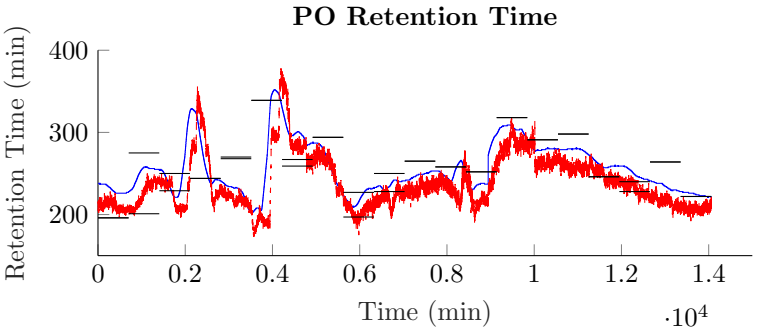

(a)

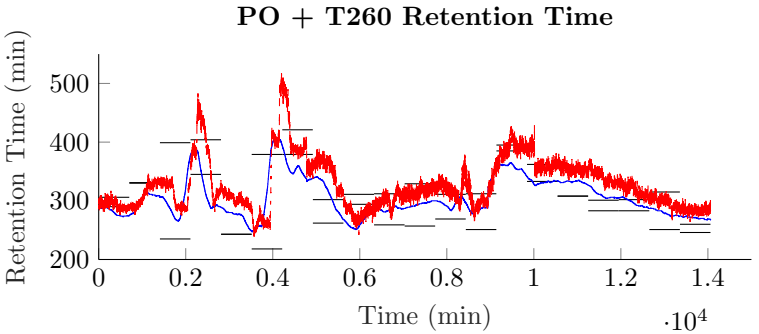

(b)

Figure 4.1 The top graph show PO retention time, while the bottom graph show the PO + T260 retention time. The simulation were done over a 6 day period. The black bars represent the ARX estimation divided evenly into 20 time periods. Blue lines show the dynamic estimation by the retention time model (described in Section 3.1) and red lines are the pre-made retention time prediction.

The results and the methods itself show that the ARX estimation is a poor way of validating the retention time model. Therefore, there is no way of knowing how accurate the estimation is. As the retention time is crucial to training and testing the brightness models, this uncertainty will unfortunately carry over and weaken their predictive ability.

4.2 Kinetic Model Simulations

Early simulations of the kinetic model showed little prediction accuracy and a very heavy computational cost. Training the model with more than 25 training data points were too time consuming and showed little to no increase in prediction accuracy. The high computational complexity of the model can be explained by the difficulty optimizing the eight parameters of the model (shown in Table 2.2). Yet, the eight parameters seemed to be not enough to accurately describe the process, as the model weren't accurate on training data points. Figure 3.2 show this inaccurate fitting on the training data points.

Figure 4.2 show the short term accuracy on completely new data. The simulation was done with a single parameter fitting on 25 data points evenly spread out over the training data set (first half).

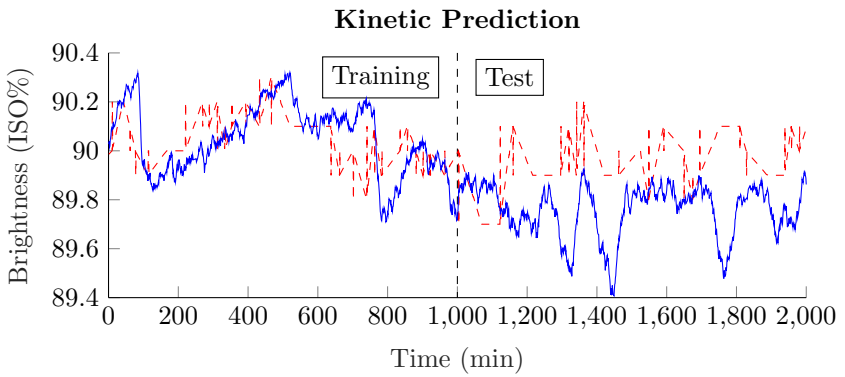

Figure 4.2 The graph (a) show a kinetic model simulation with training and test data separate. Prediction value (blue line) from the model is compared to the measurement value (red line) in both figures.

Figure 4.2 show that the kinetic model capture some of the process behaviour but misses others completely. One example of such inaccuracy is at time 1750, where the real measurement is a peak and the model predicts a valley. This, along with the poor fitting mentioned above, suggest the model is missing a significant part of the process dynamics. As was also mentioned in Section 3.4, these results

may be explained by the C_∞ parameter having fixed value in the model. Figure 3.2 showed a flat brightness curve, indicating the brightness value reaching close to the limit, which is determined by C_∞.

For the reasons mentioned, the kinetic model could potentially work better in a lower brightness range, where the C_∞ constant has a smaller effect on the process. The process should in theory be easier to model with classical parametric models. [Roberts et al., 2013] have significant success modeling the brightness gain under static conditions using a simple linear regression model. While they do not explicitly state the brightness range, they work with a lower quality recycled pulp process, which is in the lower ranges. This points to the kinetic model potentially working accurately for lower brightness pulp, where C_∞ would have a lower impact on the output brightness.

4.3 Hybrid Model Simulations

This section presents simulations done with the hybrid models described in Section 3.4, as well as a simple GPR ISO brightness model. Before the models could be simulated, parameters (described in Section 3.3) needed to be determined. Input feature selection is shown in the section below, whilst the other parameters, such as covariance kernel and training data size, can be found in Section A.2. Due to the the small ranges and large increments of the aforementioned parameters in the simulations, the results are thought to be rough and thus difficult to make an analysis. Therefore, the results in Section A.2 will not be discussed in great detail. A few points of interest are given in the section below.

Parameter Approximation

Training lengths From the data in Table A.1, it is apparent that the training data from the Big Data selection is more valuable to the GPR models than the most recent data. On the other hand, K-means selection method show no such behaviour. It is also an early indication of the poor performance of the models using K-means selection.

Smoothing The second parameter to be estimated was the moving mean filter window length. Table A.2 show that again k-means selection differs from the Big Data selection. Both, however, show improvement with the filter.

Kernel and Basis Third, the kernel and basis functions had to be estimated. As Table A.3 show, only the most common kernels and basis were tested. If there had been more time, custom functions could have been developed and tested.

Cluster Count For the K-means data selection the number of clusters used is an important part [Jiang et al., 2019]. For all three brightness models fewer clusters improved the performance, see Table A.4. This could mean that the cluster selection

when predicting is poor and chooses the wrong quite often. Therefore, fewer clusters mean less probability to choose the wrong cluster for the prediction at each time step.

One thing to note is that throughout the simulations K-means data point selection was shown to generate inconsistent results. The reason is that the k-mean clusters are built from randomly generated starting points for the centers. The training data provided to the models consists of continues sampling, thus preventing independent clusters from forming. Therefore, the k-means algorithm may not converge to similar clusters in different iterations of the simulation.

Feature Selection

The input features to be tested, shown in Table 4.1, were chosen based on availability, avoidance of redundancy and any connection to the chemical process. Some new features were created by processing existing input features. One input feature which is not included is the PO-tank retention time. In initial tests the retention time showed to be clearly detrimental to the predictive performance of the bleaching models, while showing a very low kernel scale value (large weight). This can indicate the correlation of retention time and the output to be strong and irregular. Another reason to not include the retention time is that it is an estimation. As explained in Section 3.1 the retention time estimation uses future data points and is therefore more accurate than an prediction. Obviously, the GPR models can't use future data points. For the reasons mentioned above, the retention time input feature was omitted from the simulations.

Table 4.1 Description of input features used in feature selection.

Input Feature	Description
B_{in}	ISO brightness before the PO-stage.
P_{inp}	Amount of hydrogen peroxide applied.
S_{inp}	Amount of sodium hydroxide applied.
κ	Kappa number.
T_{PO}	Temperature in the PO-tank.
F_L	Pulp fiber length before the PO-stage.
C_{PO}	Pulp concentration before the PO-stage.
B_{kin}	Kinetic prediction of brightness.
B_D	Difference between B_{in} and B_{kin}.
P_{rb}	Lower PO-tank hydrogen peroxide concentration.
P_D	Difference between P_{inp} and P_{rb}.
pH_D	Difference between lower and upper PO-tank pH.
B_{Sl}	Moving slope of B_{in} with window length 50.

As described in Section 3.3, a single GPR model was trained with data points selected over the entire data set to infer the individual kernel scales of the input

features. The training was repeated three times with a shift of data point selection and three times more with mirrored data point selection. All input features were standardized in order to avoid any scaling differences of the data. The kernel scale values were also shifted so the lowest kernel scale value were close to zero. Otherwise, difference in scaling of the kernel scales between the different GPR models could be an issue. The kernel scales of individual GPR models and their mean values for each model are shown in Figures 4.3.

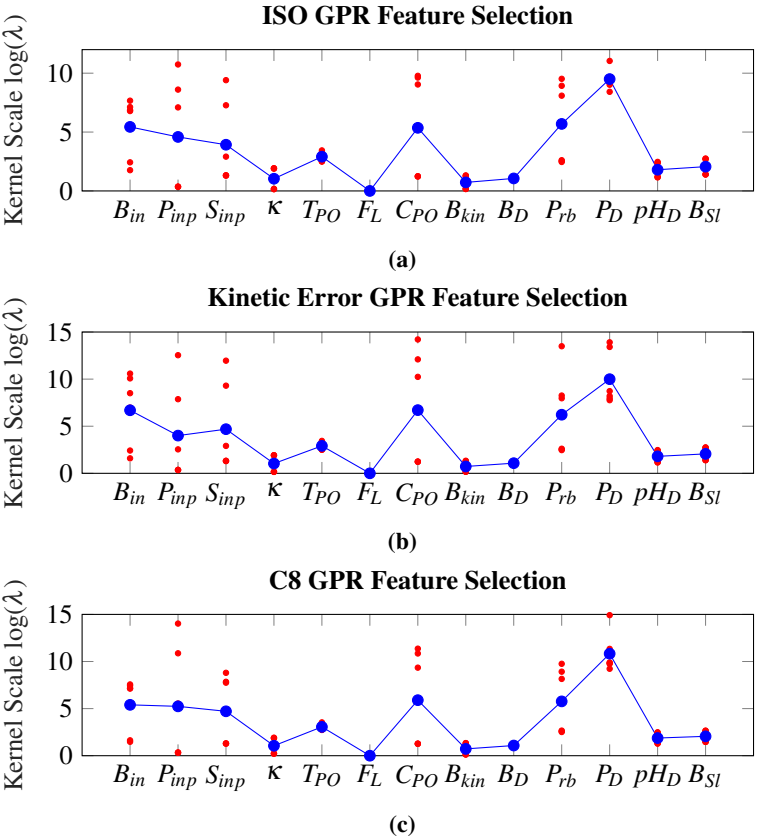

Figure 4.3 The graphs show the kernel scale of the individual input features after fitting the GPR models to their respective outputs. Shown from top to bottom: ISO GPR (a), kinetic error GPR (b) and C8 GPR (c). Red dots indicate individual trained GPR models. Blue line and dots represent their mean values.

The three figures above show a very similar pattern for the different outputs. Some of the input features have a large spread of their kernel scale, which suggests

the GPR models find strong correlations for some parts of the data and weaker for others. More iterations could have been done, but it was not deemed necessary. An interesting point is the high value of hydrogen peroxide (P_{inp}) and sodium hydroxide (S_{inp}), meaning low predictive ability for the GPR model. Obviously, P_{inp} and S_{inp} are crucial for the process; however, as the kinetic model tells us, above a certain amount the chemical dosage see a small impact on the final brightness. Data with higher variance in the chemical dosages would probably lead to more accurate GPR models. The current data has very high chemical dosage and low variance, as that is required to reach the level of brightness specified. Consequently, the GPR models do not capture the chemical dynamics of the process, and thus optimizing the chemical dosages for the ISO GPR and Kinetic Error GPR models are unfeasible. The C8 GPR is the exception as optimization can be done with the kinetic model using the predicted $\hat{C}_\infty$. As mentioned in Section 3.4, all the discrepancies of the kinetic model are estimated in $\hat{C}_\infty$.

Kappa κ A thing to note is that the kappa number κ is not measured at point A (see Figure 3.1) as all the other input features are. It is instead measured at an earlier point at the plant. Additionally, between the kappa measurement and the PO-tank, the pulp goes through several stages of bleaching and washing. Constructing a retention time model only for the kappa measurement was considered too time consuming. Therefore, the already existing retention time model was relied upon to make a rough estimate of how much shift in time the kappa measurement needed. With this in mind, the high importance the models put on the kappa measurement is surprising. This indicates the GPR models find a high correlation between the kappa measurement and output brightness, C_∞ and kinetic error. As mentioned in Section 2.1, the kappa measurement is the principal measurement in the earlier stages of the bleaching process and measures the lignin content. It is possible, therefore, that the kappa measurement provides some information on the bleachability of the chromophore groups (see Section 3.4). Part of this is what the C_∞ parameter tries to represent. This could present an easy improvement to the brightness models by adding a kappa sensor closer to the PO-tank.

Kinetic Model Prediction B_{kin} Perhaps unsurprising, the B_{kin} show a high importance with very little variance for all the models. The kinetic model should after all contain new information to the GPR models about the chemical process. So even if the C8 GPR model is not used, the kinetic model can still be an important part of modeling the PO stage.

Selection To determine the best combination of input features for the six models, test were done using the input features with the lowest kernel scale values. Then, input features were added and removed based on Figure 4.3, to find the best performing set of input features for the respective models. Table 4.2 show the chosen set of input features for each model and Table A.5 show all the test results.

Table 4.2 The chosen set of input features for each model based on Table A.5.

	Model	Inputs
Big Data	ISO GPR	K,F_L,B_{kin},B_D,pH_D,B_{SL},T_{PO}
	Kin. Err. GPR	K,F_L,B_{kin},B_D,pH_D,B_{SL},T_{PO},P_{inp}
	C8 GPR	K,F_L,B_{kin},B_D,pH_D,B_{SL}
K-mean	ISO GPR	K,F_L,B_{kin},B_D,pH_D
	Kin. Err. GPR	K,F_L,B_{kin},B_D,pH_D
	C8 GPR	K,F_L,B_{kin},B_D,pH_D,B_{SL},T_{PO},S_{inp}

Principal Simulations

The final simulations were done with all the model parameters and options determined in the previous section. Table 4.3 show the prediction performance of the six models. Most notable is the poor performance of the K-means data selection models. A possible explanation is that the amount of data available is not enough. Also likely is that basing the K-means on all the input features for the respective models (see Table 4.2) was detrimental to selecting the right cluster for predictions.

During simulations, one time period acts as the testing data set, while the other two acts as the large training data set for K-means and Big Data selection. The time periods switch places so all three are simulated as the testing data set.

Table 4.3 The final simulation results of the six models.

Data Selection	Model	RMSE
Big Data	ISO GPR	0.2282
	Kin. Err. GPR	0.2270
	C8 GPR	0.2255
K-mean	ISO GPR	0.2572
	Kin. Err. GPR	0.2446
	C8 GPR	0.2486

While Table 4.3 only show a slightly higher performance for the C8 GPR model, the tables A.1-A.5 confirms the superior performance of the C8 GPR model over the other two. It is difficult to compare these results to other similar studies as they either cover a different range of brightness, their process is not comparable or their results are not shown in detail. The remainder of this section illustrates the simulations of the Big Data C8 GPR model and analyses its performances.

Figure 4.4 show the results of a single training and prediction iteration using the Big Data C8 GPR model. The test part of the graphs is the prediction that is used when iterating over the complete data set, as to simulate the unavailability of recent data for training because of the long retention time. The top graph clearly show that the

retention is responsible for some of the difficulty of modelling the process, as the prediction deteriorates significantly over the retention time.

Graph 4.4 **(a)** showing the "true" C_∞ in red seem to have a smaller sample time than the measured ISO in red 4.4 **(b)**, however the "true" C_∞ is calculated with the smoothed measurements needed in Equation 2.3. Graph 4.4 **(b)** also show the poor resolution of the ISO brightness sensor and a few large spikes, assumed to be errors.

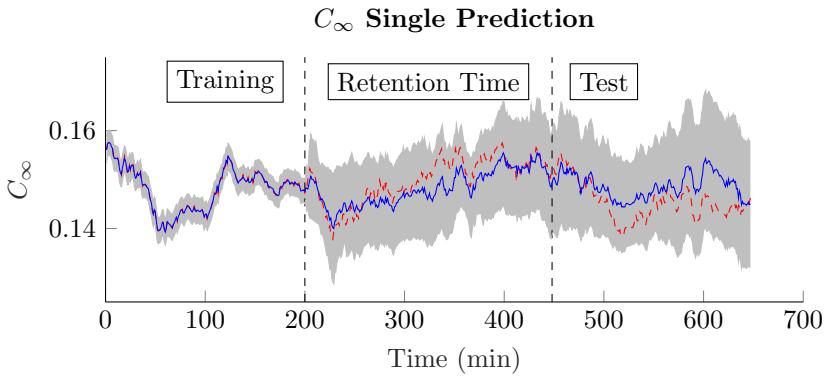

(a)

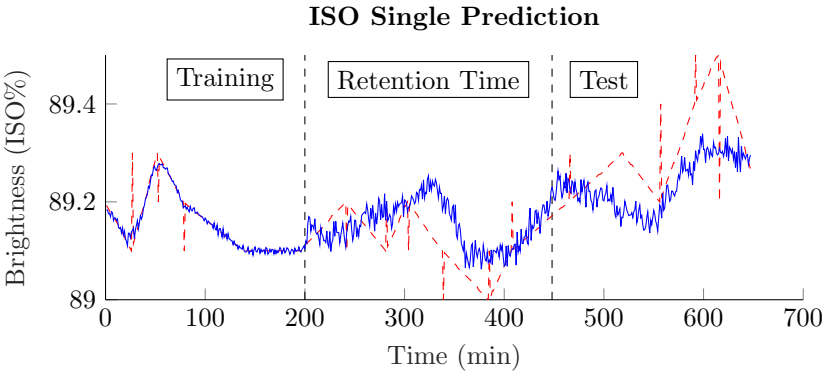

(b)

Figure 4.4 The two graphs illustrate the C_∞ (a) and brightness (b) predictions of the C8 GPR model for one iteration of training and prediction. Model prediction (blue lines) and 95% confidence interval (gray area) is compared to measured values (red lines).

Next, Figure 4.5 show the complete simulation over the three time periods using the Big Data C8 GPR model. Here the different dynamics of each time period is visible. The first time period show an accurate prediction with only a few short

outliers. The second time period have a smoother and higher ISO brightness, however the models performance is worse with longer-lasting errors. This could be due to the Big Data selection uses the other two time periods, which with their lower brightness provide poor training data for the high brightness of the second time period. The third time period show a higher variance than the previous two for both the C_∞ and ISO brightness measurement. The model, however, handles the third time period quite well considering the circumstances.

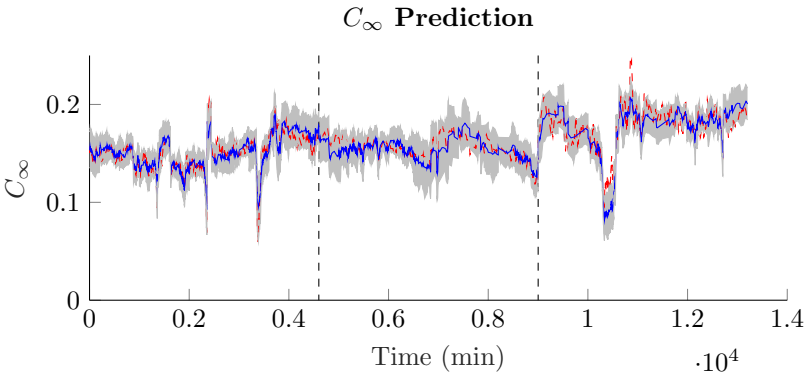

(a)

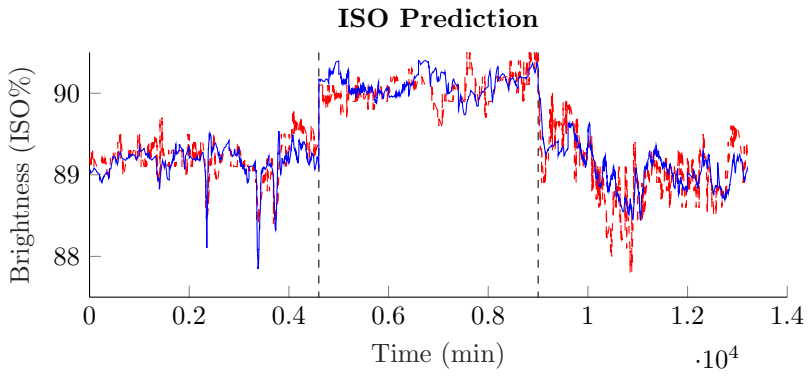

(b)

Figure 4.5 The two figures show the C_∞ (a) and brightness (b) predictions of the C8 GPR model for the complete data set. Model prediction (blue lines) and 95% confidence interval (gray area) is compared to measured values (red lines). The dashed vertical lines mark the change in data sets.

The model seem to have difficulty accurately predicting the fast changes in the brightness. Fast changes in this case are still several tens of minutes long and should

not be due to sensor noise. These fast changes can be due to a number of other reasons. The main one is differences in chemical properties of the pulp changing fast, as the pulp is only mixed in smaller quantities. Another reason could be faults in the previous bleaching stages which could lower the brightness significantly.

Chemical Optimization

In this section the optimization simulations are presented for the goal attainment method, as explained in Section 3.5, applied on the C8 GPR model. Three objective functions were set up for the algorithm: The brightness prediction from the kinetic model with the predicted C_∞, total dosage of $[H_2O_2]$ and $[OH^-]$ as inputs to the kinetic function. Each of the objective functions had a goal and weight $\mathbf{w}$. The brightness goal was 89 ISO%, and the chemical goals were 0.0253 and 0.0183, which is half of their original mean values. The weights could then be adjusted to under- or overachieve these goals. The weights were defined as

$$\mathbf{w} = \begin{pmatrix} w_B \\ 1.3849 \\ 1 \end{pmatrix}. \tag{4.2}$$

The first row is the brightness weight and other two are the chemical weights. The chemical weights are fixed to the same relation as distance from their mean measured values to their set goals. Consequently, the algorithm treats the $[H_2O_2]$ and $[OH^-]$ dosages as equally costly. The next step is to determine w_B, which decides the importance of saving chemical versus reaching the goal brightness.

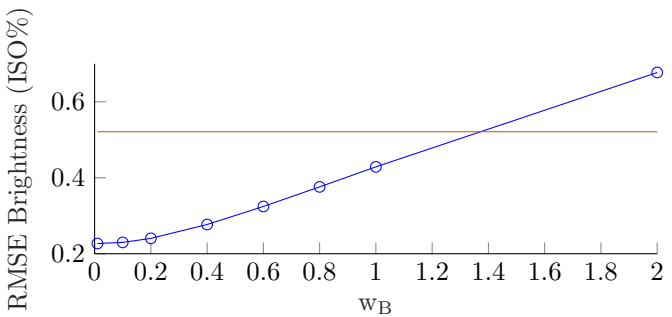

Figure 4.6 Evaluation of the objective function values used in the optimization for different weights w_B. The RMSE of the estimated and goal brightness of 89.5% is shown in the figure. The red line show the original measured value and the blue line represent the optimized values.

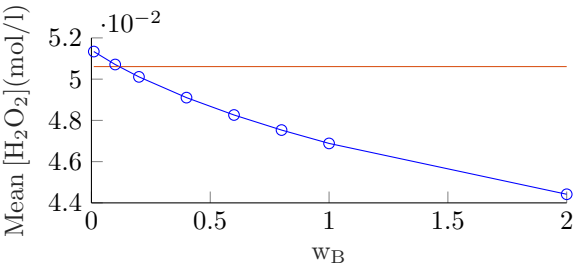

(a)

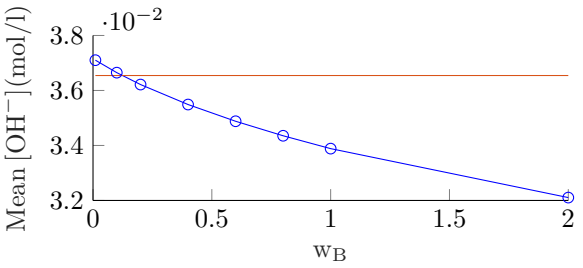

(b)

Figure 4.7 Evaluation of the objective function values used in the optimization for different w_B. Figures (a) and (b) presents the mean chemical dosages. Red lines are the original measured values and blue lines are the optimized values.

From the graphs in Figure 4.6 and 4.7 we can see a large improvement in reaching the goal brightness while saving chemicals at a low w_B. The most likely explanation is that too much chemicals were used in the original measured data. Later, Figure 4.8 clearly show excessive amounts of chemicals were used in the middle third of the simulations. As previously mentioned, the two chemical dosages were treated as equally expensive to algorithm. However, this can be modified to adjust for other ambitions. For example, they could be adjusted for their respective financial costs or environmental impact.

Choosing the proper weight w_B is not straightforward and mostly up to the user. For the following simulations w_B was chosen as 0.4, which according to Figure **??** has a very low brightness error and still saves chemicals. Figure 4.8 presents the results of the optimization.

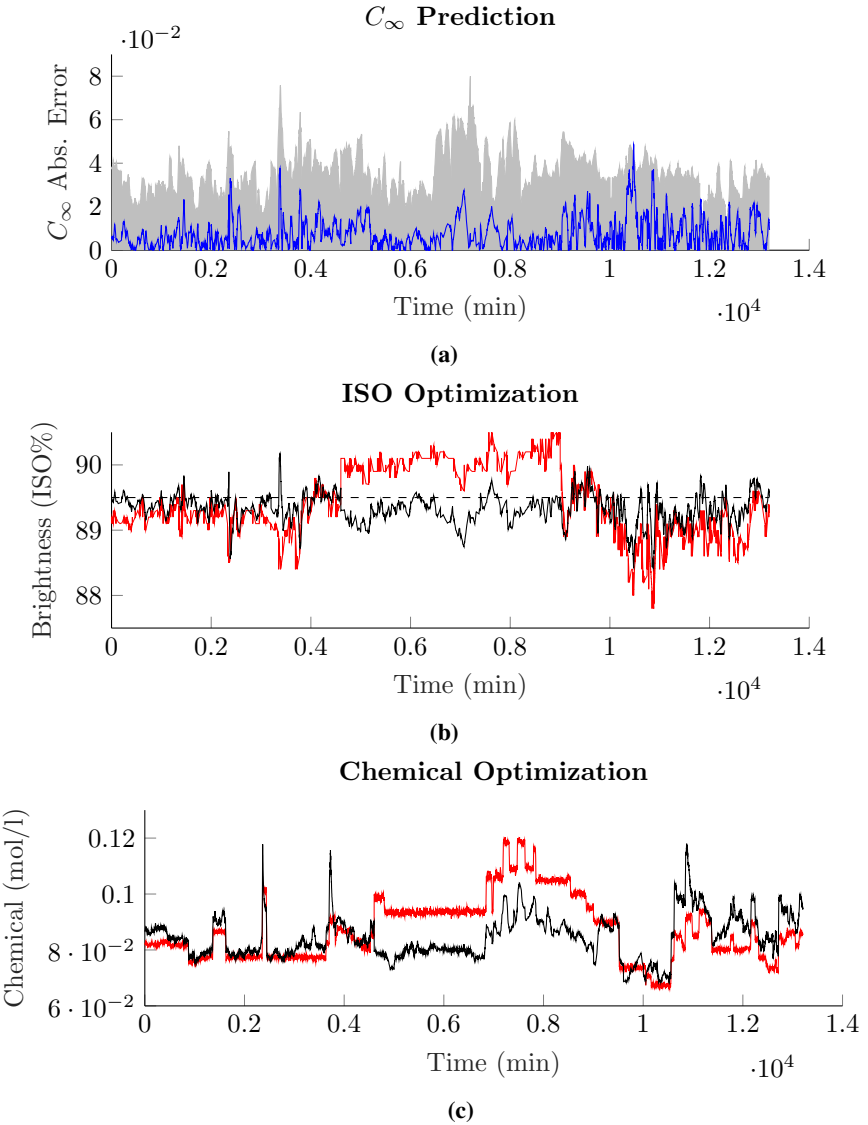

Figure 4.8 The three figures show the results from optimizing the bleaching process using the C8 GPR model for prediction and $w_B = 0.4$. The top figure (a) show the absolute C_∞ prediction error (blue line) and the 95% confidence interval of the C8 GPR model. The middle figure (b) show the estimated ISO brightness after optimization (black line) and originally measured (red line). The bottom figure (c) show the total chemical dosage ($[H_2O_2] + [OH^-]$) after optimization (black line) and originally measured (red line).

An obvious thing is the relation of C_∞ prediction error and ISO optimization error. It is impossible for the optimization algorithm to work perfectly without a perfect model. This is hard to avoid unless a different control strategy is implemented. Nonetheless, it can be seen that the optimization do improve the brightness to be closer to 89.5%, while saving chemical costs. A pattern of the optimization is that the brightness is optimized to be slightly below 89.5%, which is a consequence of also trying to save chemicals at the same time. If it is very important that the brightness is above a brightness threshold, the weights can be adjusted accordingly.

A possibility to improve the optimization is to implement a control rule based on the confidence interval of the prediction [Yang and Maciejowski, 2015]. The figure show that the prediction confidence interval size and prediction error correlate for the most part. Adjusting the control based on the uncertainty of the model is not something new, but there was not enough time to implement it in this thesis.

4.4 Limitations and Implementation Challenges

In this section the limitations of the simulations/models and the challenges of implementing them at a plant, are discussed.

- The testing time periods were selected to have all the measurements available, which is not always the case. Missing just one input to the models will disrupt the brightness prediction completely. This shows the need for adding robustness to the prediction models.
- The retention time were an estimation instead of a prediction. As there is no access to the future pulp flow data, the estimation presented in this thesis cannot be implemented. This mostly affects the kinetic model and in turn the C8 GPR model.
- Hardware requirements for the simulations are low, as they were conducted on a laptop. Also, as shown in the simulations the process is very slow so there is ample time to both make predictions and model training in a real-time setting. However, if the training sizes for the GPR are greatly increased, training time could present a problem.
- The optimization results are not conclusive as they are themselves an prediction from the kinetic model with the C_∞ solution. To avoid this, the optimization would have be implemented on the real process.

5

Conclusions

The aim of this thesis was to model and optimize the brightness of the PO bleaching process, see 1.2. I think the modelling goals were mostly reached with some interesting results. The kinetic model could have been tested in greater detail, especially with different fitting methods. But I believe it was studied enough to conclude a poor performance for this process. The optimization part, however, was not studied as thoroughly and diverged from optimization implementations in previous studies. But as the optimization aim stated, the optimization was more to show the potential and application of the model. The following part highlights some key takeaways from this thesis.

The kinetic model is not sufficient on it's own, which probably is caused by the C_∞ parameter being time variant. However, the kinetic model can improve the GPR models by making a hybrid model or as an input feature. Also validating the reasons why the kinetic model failed, the GPR found the input brightness and especially the chemical dosages to be poor predictors for the output brightness, which the kinetic model depend on. Instead, the GPR model found that the output brightness correlated more with the kappa and fiber length measurement, which can provide information of the chemical properties of the pulp. The GPR models infers some of the chemical properties of the pulp to predict the output brightness. However, more sensors measuring chromophore groups or other chemical properties are needed to develop accurate models. This points to the potential of the GPR models as more inputs can simply be added without having to redevelop the model for the new inputs.

5.1 Future Work

This section lists some of the more interesting parts of the thesis that require further studying.

- As the GPR models can handle more input features than tested in this thesis, adding more inputs from earlier parts of the plant would be of interest. Thus, the model can possible infer the chemical properties better by obtaining

data from several bleaching stages. The only implementation challenge is the amount of data and the multiple time-variant retention times.

- More advanced data selection methods for training the GPR models could benefit the performance greatly, as the results showed very poor performance with poor training data. This can also include improving the K-means clustering with more data and better selection.
- More variation of the chemical dosages of the training data could help the models to capture a greater range of the process dynamics. The GPR should also find the chemical dosages more useful, and thus the GPR models could be optimized.
- The optimization of bleaching chemicals and control of the brightness needs to be studied further before implementation on the real process is viable. Especially, the robustness of the optimization/control.
- Adding a kappa sensor before the PO-tank and brightness, peroxide sensors along the PO-tank would be interesting and could benefit the models greatly. It could also help gain a greater understanding of the bleaching dynamics.

A

Appendix

A.1 Kinetic Simulations

A.2 Model Simulations

Presented below are tables showing the results from simulations done in order to determine appropriate parameters and features for the models. The tables are shown in order in which the parameter and features were determined. Therefore, simulations shown in one table uses the optimal parameters and features for the models from the tables above it. Performance is measured by the RMSE of the ISO brightness. The lowest value for each model and table have their table cell marked in grey.

Table A.1 The table show the ISO RMSE of model simulations to determine appropriate sizes of the training data set. N_{Re} is the size of the retraining data set, while N_{Sel} is the size of the Big Data training set or the cluster size of K-means clustering. Simulations with a total training size of more than 600 were not done as they would be too time consuming. For the simulations the moving mean window was set to 160, the covariance kernel was ardexponential and the basis function was linear.

		Big Data			K-means		
	$N_{Re} \setminus N_{Sel}$	200	300	400	200	300	400
ISO GP	200	0.2716	0.2698	0.2692	0.3792	0.3788	0.3747
	300	0.2800	0.2777	∼	0.3296	0.3483	∼
	400	0.2732	∼	∼	0.3295	∼	∼
Kin.Err. GP	200	0.2710	0.2690	0.2688	0.3870	0.3926	0.3956
	300	0.2785	0.2763	∼	0.3338	0.3157	∼
	400	0.2710	∼	∼	0.3617	∼	∼
C8 GP	200	0.2716	0.2691	0.2679	0.4496	0.4542	0.4382
	300	0.2812	0.2772	∼	0.4273	0.4039	∼
	400	0.2752	∼	∼	0.4086	∼	∼

Table A.2 The table show the ISO RMSE of model simulations to determine appropriate smoothing mean window length of the data. N_{Wind} is the size of the mean window. Training set sizes were set to the lowest RMSE from A.1 for the respective models. The covariance kernel was ardexponential and the basis function was linear.

	Big Data			K-means		
N_{Wind}	ISO GP	Kin.Err. GP	C8 GP	ISO GP	Kin.Err. GP	C8 GP
1	0.2485	0.2505	0.2485	0.3032	0.3524	0.3814
5	0.2370	0.2363	0.2324	0.3191	0.3372	0.3598
10	0.2331	0.2324	0.2312	0.3099	0.3258	0.3407
20	0.2389	0.2409	0.2406	0.2966	0.3263	0.2815
40	0.2544	0.2559	0.2566	0.3360	0.3007	0.2893
80	0.2855	0.2855	0.2791	0.3847	0.3663	0.3680
120	0.2838	0.2823	0.2743	0.4365	0.3561	0.4654
160	0.2834	0.2821	0.2754	0.3542	0.3396	0.4537

Table A.3 The table show the ISO RMSE of model simulations to determine appropriate covariance kernel and basis function of the GPR model. On the horizontal axis are the basis functions: none, constant and linear. The vertical axis contain the covariance kernels: squared exponential (SE) and exponential (E). Training set sizes and smoothing window length were set to the lowest RMSE from Table A.1 and Table A.2 for the respective models.

		Big Data			K-means		
	Kern.\Bas.	none	const.	lin.	none	const.	lin.
ISO GP	E	0.2311	0.2306	0.2331	0.3004	0.2756	0.3181
	SE	0.4876	0.4586	0.2509	19.5901	0.3008	0.3056
Kin.Err. GP	E	0.2334	0.2332	0.2324	0.3297	0.3402	0.3265
	SE	0.3497	0.3308	0.2495	0.4010	0.3652	0.3099
C8 GP	E	0.2309	0.2309	0.2312	0.3074	0.2982	0.2893
	SE	1.0011	0.3359	0.2489	1.2438	0.3767	0.3024

Table A.4 The table show the ISO RMSE of model simulations to determine appropriate covariance kernel and basis function of the GPR model. On the horizontal axis are the basis functions: none, constant and linear. The vertical axis contain the covariance kernels: squared exponential (SE) and exponential (E). Training set sizes and smoothing window length were set to the lowest RMSE from Table A.1 and Table A.2 for the respective models.

	K-means		
N_{Clust}	ISO GP	KinErrGP	C8 GP
3	0.2432	0.2474	0.2839
6	0.2364	0.2704	0.2780
9	0.2478	0.3018	0.2864
12	0.2969	0.2537	0.2975

Table A.5 The table show the ISO RMSE of model simulations to determine the optimal input features used in the GPR input. The second colon contains the input features, descibed in Table 4.1, used in the simulation. Training set sizes, smoothing window length, kernel and basis function were set to the lowest RMSE from Table A.1-A.3 for the respective models.

Model	Input Features	RMSE
Big Data		
ISO GPR	K,F_L,B_{kin},B_D,pH_D,B_{SL}	0.2289
	K,F_L,B_{kin},B_D,pH_D,B_{SL},T_{PO}	0.2282
	K,F_L,B_{kin},B_D,pH_D,B_{SL},T_{PO},S_{inp}	0.2285
Kin. Err. GPR	K,F_L,B_{kin},B_D,pH_D,B_{SL}	0.2286
	K,F_L,B_{kin},B_D,pH_D,B_{SL},T_{PO}	0.2284
	K,F_L,B_{kin},B_D,pH_D,B_{SL},T_{PO},P_{inp}	0.2270
	K,F_L,B_{kin},B_D,pH_D,B_{SL},T_{PO},P_{inp},S_{inp}	0.2273
C8 GPR	K,F_L,B_{kin},B_D,pH_D	0.2271
	K,F_L,B_{kin},B_D,pH_D,B_{SL}	0.2255
	K,F_L,B_{kin},B_D,pH_D,B_{SL},T_{PO}	0.2289
K-means		
ISO GPR	K,F_L,B_{kin},B_D	0.2686
	K,F_L,B_{kin},B_D,pH_D	0.2572
	K,F_L,B_{kin},B_D,pH_D,B_{SL}	0.2763
	K,F_L,B_{kin},B_D,pH_D,B_{SL},T_{PO}	0.2727
Kin. Err. GPR	K,F_L,B_{kin},B_D	0.2800
	K,F_L,B_{kin},B_D,pH_D	0.2446
	K,F_L,B_{kin},B_D,pH_D,B_{SL}	0.2466
	K,F_L,B_{kin},B_D,pH_D,B_{SL},T_{PO}	0.2671
C8 GPR	K,F_L,B_{kin},B_D,pH_D,B_{SL}	0.2757
	K,F_L,B_{kin},B_D,pH_D,B_{SL},T_{PO}	0.2563
	K,F_L,B_{kin},B_D,pH_D,B_{SL},T_{PO},S_{inp}	0.2486
	K,F_L,B_{kin},B_D,pH_D,B_{SL},T_{PO},S_{inp},P_{inp}	0.2935

Bibliography

Alberth, L. (2011). “Experimentell studie av kinetiken för peroxidblekning av pappersmassa”. **4**:9.

Chen, N., Z. Qian, I. Nabney, and X. Meng (2014). “Wind power forecasts using gaussian processes and numerical weather prediction”. *Power Systems, IEEE Transactions on* **29**, pp. 656–665. DOI: 10.1109/TPWRS.2013.2282366.

Coleman, T. F. and Y. Li (1996). “An interior trust region approach for nonlinear minimization subject to bounds”. *SIAM Journal on Optimization* **6**:2, pp. 418–445. DOI: 10.1137/0806023. eprint: https://doi.org/10.1137/0806023. URL: https://doi.org/10.1137/0806023.

Coleman, T. and Y. li (1994). “On the convergence of reflective newton methods for large-scale nonlinear minimization subject to bounds”. *Math. Program.* **67**, pp. 189–224. DOI: 10.1007/BF01582221.

Dence, C. and D. Reeve (1996). *Pulp Bleaching – Principles and Practice*. TAPPI Press, Atlanta, USA.

Gembicki, F. and Y. Haimes (1975). “Approach to performance and sensitivity multiobjective optimization: the goal attainment method”. *IEEE Transactions on Automatic Control* **20**:6, pp. 769–771.

Guyon, I. and A. Elisseeff (2003). “An introduction to variable and feature selection”. *J. Mach. Learn. Res.* **3**, pp. 1157–1182. ISSN: 1532-4435.

Jiang, S., X. Shen, and Z. Zheng (2019). “Gaussian process-based hybrid model for predicting oxygen consumption in the converter steelmaking process”. *Processes* **7**, p. 352. DOI: 10.3390/pr7060352.

Lenz, H., J. Horn, T. Runkler, M. Dinkel, T. Schmidt, A. Sieber, and V. Mickal (2005). “Modelling of peroxide-bleaching of pulp using gaussian processes”. *IFAC Proceedings Volumes* **38**:1, pp. 489–494.

López Jaimes, A., S. Zapotecas-Martínez, and C. Coello (2011). “An introduction to multiobjective optimization techniques”. In: pp. 29–57. ISBN: 978-1-61122-818-2.

Malmberg, B. (2006). “Development and application of general process simulation tools within the pulp and paper industry”. *PhD Dissertation*.

Mota, S., M. Carvalho, and L. Ferreira (2007). “Pressurized hydrogen peroxide bleaching of eucalyptus globulus pulps. part ii: kinetics”. *Nordic Pulp and Paper Research Journal* **22**, pp. 23–27.

Peter, F. and H. Manfred (2006). “The mathematical model of mechanical pulp bleaching process”. *IFAC Proceedings Volumes* **39**:14, pp. 70–75.

Rasmussen, C. E. and C. K. I. Williams (2006). *Gaussian processes for machine learning*. Cambridge, Mass. : MIT Press, cop. 2006. ISBN: 026218253X.

Roberts, S., M. Osborne, M. Ebden, S. Reece, N. Gibson, and S. Aigrain (2013). “Gaussian processes for timeseries modelling”. *Phil. Trans. R. Soc. A.* **371**. DOI: 10.1098/rsta.2011.0550.

Taylor, J. and K. Akida (2007). “Indirect adaptive model predictive control of a mechanical pulp bleaching process”. In: vol. Montreal, Canada.

Teder, A. and D. Tormund (1980). “The equilibrium between hydrogen peroxide and the peroxide ion – a matter of importance in peroxide bleaching”. *Svensk papperstidning* **4**.

Yang, X. and J. Maciejowski (2015). “Fault tolerant control using gaussian processes and model predictive control”. *International Journal of Applied Mathematics and Computer Science* **25**. DOI: 10.1515/amcs-2015-0010.

Lund University
Department of Automatic Control
Box 118
SE-221 00 Lund Sweden

Document name
MASTER'S THESIS

Date of issue
December 2020

Document Number
TFRT-6120

Author(s)
Jonas Christensen Strömgren

Supervisor
Sara Ingves, Södra Cell, Sweden
Tore Hägglund, Dept. of Automatic Control, Lund University, Sweden
Kristian Soltesz, Dept. of Automatic Control, Lund University, Sweden (examiner)

Title and subtitle
Modelling and Optimization of Peroxide Pulp Bleaching Process

Abstract

The wood pulp industry has been around for a long time, but new higher quality pulp require more advanced solutions to old processes. One of these processes is the peroxide (PO) bleaching process, which is the last of a whole chain of bleaching processes at the Mörrum pulp processing plant. The aim of this thesis was to develop and study a model for the peroxide pulp bleaching process, and thereafter optimize the process with the model. The PO-stage is a multivariable, non-linear process with a variable retention time of a few hours. The models tested was a kinetic reaction model, a Gaussian process regression (GPR) model and hybrid models of the two. Before the models could be tested a retention time estimation model was made to compensate for the variable retention time. The bleaching simulations showed the kinetic model could not accurately model the brightness output. The kinetic lacked variability in the maximum brightness parameter C∞. However, the combination of estimating C∞ for the kinetic model with an GPR model proved to be a good performing model. Prediction on slow brightness changes was accurate, but fast changes was harder and large error could occur. The optimization of the hybrid model showed that chemical dosages could be lowered while achieving a smoother and more precise brightness. Further studies on robustness of the brightness model and the optimization model are needed before implementation on the real process can be done.

Keywords

Classification system and/or index terms (if any)

Supplementary bibliographical information

ISSN and key title
0280-5316

ISBN

Language
English

Number of pages
1-48

Recipient's notes

Security classification

http://www.control.lth.se/publications/